Nineteenth Australasian Wind Engineering Society Workshop, April 4-6, 2018, Torquay, Victoria

Antenna Shielding on Monopole Structures - Part 2 Computational

Tom Moyle[1], Richard Jones[2], Neil Mackenzie[3]

[1]*Aurecon Group, Adelaide, SA, thomas.moyle@aurecongroup.com*

[2]*Aurecon Group, Adelaide, SA,* richard.jones@aurecongroup.com

[3]*Aurecon Group, Adelaide, SA,* neil.mackenzie@aurecongroup.com

ABSTRACT

This paper will outline the second part of the antenna shielding study undertaken by Aurecon. A calibrated computational fluid dynamics (CFD) method was developed enabling calculation of the effective sail areas (ESA) for headframe and antenna configurations that were not included in the experimental testing regime. The computational method has been included in an update of the "Deployment Rules for Telstra Antenna Support Structures", ensuring a consistent approach to antenna shielding is taken by Telstra's structural contractors. The paper will discuss the CFD implementation, calibration factors, and other findings.

1. Introduction

This paper should be considered as a direct continuation of the preceding paper titled "Antenna Shielding on Monopole Structures – Part 1 Experimental" (Moyle et al., 2018).

2. CFD Considerations

CFD is the use of applied mathematics, physics and computational science to analyse fluid flows. The governing equations for motion of a fluid media is governed by the combined actions of the continuity and momentum equations, together with the energy equation. The physical properties of the problem under investigation often lead to simplifications to these governing equations, enabling faster computation of their solution. Key drivers in the choice of method and subsequent simplifications include the physics of the problem together with engineering and commercial requirements.

As the end goal of the research was the development of a computational method available to Telstra's structural contractors, it was required that:

- The mesh size must allow solution with an average engineer's desktop computer memory.
- Computational time must not be overly costly with an average engineer's desktop computer speed.
- The meshing strategy, choice of numerical discretisation and matrix solvers must be robust to avoid specialist intervention.
- The CFD method must be implemented with an open source tool such that software licensing does not prevent the contractor from performing the analysis.

Consequentially the open-source CFD software OpenFOAM was used to solve the steady solution of the governing equations. The time dependent solution of the governing equations is not feasible given the above restrictions.

3. CFD Application

Given the low Mach number flows in near-ground atmospheric boundary layer flow, the governing equations solved in the CFD model are the incompressible Navier-Stokes equations with constant laminar viscosity. Turbulence closure and hence turbulent viscosity is provided by the kOmegaSST turbulence model (Menter and Esch, 2001).

A Reynolds Averaged Navier Stokes (RANS) steady solution of these governing equations is considered in this research as the solution method must be tractable for Telstra's contractors to implement in practice. The numerical implementation is the finite volume method on a co-located, hexahedral dominant mesh. The Semi-Implicit Method for Pressure-Linked equations (SIMPLE) approach (Patankar, 1980) is used for pressure-velocity coupling and the segregated equations are solved with the Gauss-Seidel family of matrix solvers.

Each term in the set of equations was discretised on the finite volume using the following approaches:

- All gradient terms by linear (central) second order and cell limited for boundedness;
- Divergence of momentum by linear-upwind, blended in each direction for stability (second order as convergence is approached);
- All remaining divergence terms by upwind to ensure boundedness of turbulent variables;
- All Laplacian terms by linear (central) second order;
- All interpolations from cell faces to cell centres were linear (central) second order;
- All surface normal gradients were corrected for non-orthogonality by including a limited explicit gradient component.

The wind tunnel test freestream turbulence intensity was less than 1.2% for z > 600mm and has a maximum of 4% for 300mm ≤ z < 600mm. To replicate this flow freestream turbulence was modelled with a minimum turbulent kinetic energy of k=0.24 m^2/s^2 and a turbulent dissipation frequency of 1.78 Hz. These values correspond to a freestream turbulence intensity of approximately 2% with a length scale of 0.5m. This 2% turbulence intensity flow was applied at the domain inlet, in addition to acting as minimum values throughout the flow field.

The computational domain was created to match the cross-sectional area (2m x 2m) to the wind tunnel. The leading fetch was set to 2m upstream of the CAD model, while the outlet was set 4m downstream. The meshing strategy is intended to balance accurate solution of flow field effects with the expected computational resources of the average engineering contractor. Cell sizes ranged from cubes of 100mm edge length down to 3mm edge length in the near field flow. Inflation layers are added immediately adjacent the body surface with a cell height of 1.4mm. The resultant y^+ values are typically less than 30 on the antenna/headframe surfaces which is appropriate for the Reynolds averaged kOmegaSST turbulence model and continuous wall functions.

A CAD model of each headframe was created at scale and mounted on a pole of 3125mm length. For the CFD simulations each of these frames were reduced to 1:5 scale and each component placed as per the wind tunnel scenario. The surface of the headframe and pole geometry were treated as a rough wall to mimic the 40 grit sandpaper used in the wind tunnel testing. Here a standard wall roughness model was used with surface roughness height coefficient, $k_s = 420 \times 10^{-6}$ m and tuning parameter of $C_s = 0.5$.

Boundary conditions were standard choices for external aerodynamic problems and are listed in Table 1. Scalar variables undergoing transport such as velocity, turbulent kinetic energy and dissipation frequency are fixed at inlet boundaries and a zero gradient is assumed at outlet boundaries. Of note is the use of the inletOutlet on the scalars and pressureInletOutletVelocity on the velocity vector at the outlet. These boundary conditions apply the above rubric when the flux on the outlet faces out of the

domain; however, for faces where inflow is predicted due to wake induced flow effects the boundary condition switches to a fixed value inflow with velocity magnitude estimated from the pressure field. This combination of outlet conditions helps stabilise the numerical solution during convergence.

The turbulent viscosity field, ν_t, is calculated by the kOmegaSST turbulence model on all cells and boundaries except the boundary faces that comprise a solid wall surface. Here a wall function applies, in this case the standard wall function based on the turbulent kinetic energy variable, k. The corresponding turbulent variables on these boundary faces are specified with the kqRWallFunction (zero gradient) and omega wall function.

The use of slip boundaries on the sides of the domain allows for the tangential flow of velocity with no flux normal to the faces which can impose blockage effects on the flow field in a similar manner to a wind tunnel.

Table 1: Summary of boundary conditions.

	Inlet	**Outlet**	**Sides**	**Walls**
k	fixedValue	inletOutlet	Slip	kqRWallFunction
ω	fixedValue	inletOutlet	Slip	omegaWallFunction
$\vec{U}$	fixedValue (20m/s)	pressureInletOutletVelocity	Slip	fixedValue (0 0 0)
p	zeroGradient	fixedValue (0 relative)	Slip	zeroGradient
ν_t	calculated	calculated	calculated	nutkRoughWallFunction

4. Calibration

CFD is good at modelling trends and changes in body forces due to changes in design or direction of the flow. However, to determine absolute body forces CFD should be calibrated against wind tunnel results. In some industries, CFD predictions are calibrated against wind tunnel measurements by a calibration offset,

$$\mathrm{ESA}_{CFD} + \mathrm{offset} \cong \mathrm{ESA}_{WT} \tag{1}$$

Here the offset is assumed constant for all variations on an existing design, which typically holds true if geometrical variations are moderate. This approach was initially explored; however, the large changes in geometry between headframe types eliminated the possibility of a constant calibration offset across the headframe types.

Instead, a wind tunnel calibration factor, α, has been formulated as follows

$$\alpha(S) \cdot \mathrm{ESA}_{CFD} \cong \mathrm{ESA}_{WT} \tag{2}$$

Where α was determined using a multi-variate ordinary least squares regression algorithm (Scikit-learn developers, 2017). Several formulations for α were considered including linear coefficients of the frontal area, frontal area as a ratio of an empty headframe, absolute width, and angle of incidence. The final formation was a simple linear function of the frontal area S,

$$\alpha(S) = C_1 + C_2 \cdot S \tag{3}$$

The key purpose of this work is to accurately estimate the maximum loading on a headframe configuration. Therefore, when formulating the CFD calibration factor a focus was placed on calibrating against the maximum ESA from wind tunnel tests, rather than matching the ESA prediction across all angles of incidence.

Given this objective, the maximum ESA for each headframe configuration was identified and the ratio between wind tunnel and CFD results used as the target for the multi-variate ordinary least squares regression fit. For calibrating the correction factor, the RRU mount and the Lattice headframes were excluded from the regression fit target set due to the inconsistent performance of the steady CFD method for these geometries. Identification of coefficients C_1 and C_2 resulted in

$$\alpha = 1.1825 - 0.2655 \cdot S \tag{4}$$

Where C_1 and C_2 remain constant across the headframe types. For these coefficients r^2=0.996 for the maximum ESA across the target set of headframes while r^2=0.976 when considering ESA across all angles of incidence. The calibration of CFD predicted ESA results to wind tunnel experiments was conducted prior to application of a blockage correction. The calibration factor, α varied from 1.03 to 1.23. The raw CFD results were always lower than the corresponding wind tunnel measurement.

5. Observations

The solution of the steady-state governing equations is appropriate where the physical behaviour of the fluid flow does not exhibit large transient behaviour. Given the large-scale vortex shedding that occurs in the wake of individual bluff body geometries (Figure 1C), convergence of the steady solution for individual antennas and components did not always occur (Figure1A, Figure 1B). For groups of bluff bodies, such as a headframe with attached antennas and components, it was found that typically the combined interference of several bodies disrupted large-scale transient behavior, such that convergence to a steady mean flow field was not significantly disrupted. This was found to be a function of headframe geometry and effected the agreement between the wind tunnel and CFD along-wind ESA. The triangular headframes (M1 with and without cross arms, Rocla, and J1/J2) had strong agreement; the Square headframe had adequate agreement; and the RRU mounts and circular headframes (Circular, Lattice, and Mercedes) had low agreement. The RRU mounts and circular headframe geometries performed poorly as the physical flow fields induced large scale velocity fluctuations that violated the underlying steady assumption used in this CFD method. A transient CFD method is required to adequately resolve the physical flow field about these headframes. However, given the difficulty of performing transient CFD simulations in a commercial context a transient calibrated method was not developed in this research for these headframe geometries. If adequate agreement was not found between the wind tunnel and CFD results for a similar headframe this CFD method should not be used and further wind tunnel testing or conventional conservative analysis methods must be employed.

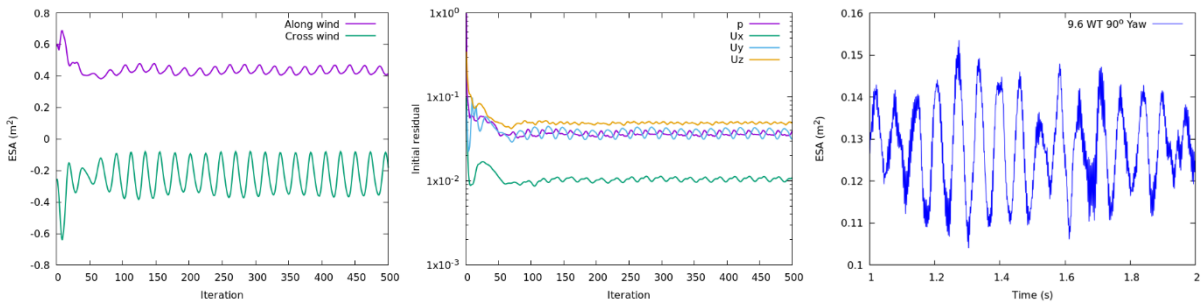

Figure 1: [Left (A)] - Uncorrected ESA and residuals, [Centre (B)] - against iterations for the VVPX310 antenna at 50° yaw, [Right (C)] - Experimental ESA of the RRU mount against time.

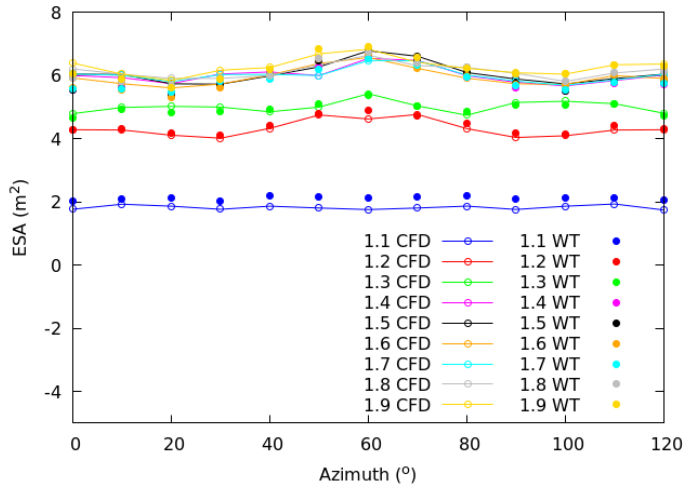

Config.	WT std. dev. (%ESA)	CFD Error (%)
1.1	12.3	-11.7
1.2	5.7	-2.8
1.3	7.3	1.0
1.4	4.7	-0.4
1.5	7.4	0.5
1.6	4.6	-1.4
1.7	5.2	-1.0
1.8	5.6	-1.7
1.9	4.6	-1.4

Figure 2: M1 experimental and calibrated CFD results, experimental standard deviation, and computational error.

6. Deployment Rules & Workflow

If the structure and its footing load are over capacity using conventional analysis methods the structural contractor is to implement the presented work. They are to:

- use the experimentally determined ESA data if it exists for the headframe/antenna configuration or,
- complete a CFD analysis using the CFD template and Telstra CFD Guidelines developed by Aurecon for Telstra.

Following either of the above if the structural capacity is still exceeded after considering load reduction strategies (e.g. retrieval of redundant equipment), the structural contractor can proceed to recommend strengthening or swap-out of the structure.

Given the uncertainties discussed previously due to the experimental method, transient effects, and discrepancies between real-world installations and their drawings the user has been given the following guidelines for applying the results:

- If the results do not show evidence of transient effects and there are strong validation results against wind tunnel data for a similar headframe configuration, the user is advised to apply a 10% safety factor to the maximum corrected ESA calculated by the CFD model.
- If the validation to wind tunnel data is only moderate or there is minor evidence of transient effects in the ESA then a safety factor of at least 15% is recommended.
- If there is weak evidence that the CFD predictions can recreate wind tunnel test data or if there is clear evidence of transient effects in the results then the user is advised to conduct wind tunnel testing or accept a drag estimation from traditional methods.

6. Conclusions

Strong agreement between CFD and wind tunnel results were found for all configurations with the M1, Rocla and J1/J2 headframe type. This suggests the CFD simulation and the correction methods outlined in this report adequately predict along-wind ESA for these headframe types when loaded with components. Adequate CFD predictions of maximum along-wind ESA were found for the Square headframe configurations. The physical flow field for the Circular, Lattice, RRU mount, and Mercedes

headframes induced large scale velocity fluctuations that violated the underlying steady assumption used in the CFD method. Consequently, CFD predictions did not adequately agree with wind tunnel tests for these headframes. In this circumstance the steady CFD solution is inadequate and a transient CFD method is required to accurately resolve the flow field. This has been reflected in the Telstra CFD Guidelines. The safety factor given in the Telstra CFD Guidelines is selected dependent on the presence of transients in the solution and if there is evidence of a similar headframe configuration having strong validation results with the corresponding wind tunnel study. If strong transients are present in the CFD results it is required that a conventional conservative method to estimate the drag is used or a wind tunnel test is performed.

Acknowledgement

Aurecon would like to acknowledge our client, Telstra for the opportunity to carry out these works and present the findings of our research.

References

Menter, F.R., and Esch, T., 2001, "Elements of Industrial Heat Transfer Prediction", 16th Brazilian Congress of Mechanical Engineering (COBEM).

Moyle, T., Mackenzie, N., Jones, R., 2018, "Antenna Shielding on Monopole Structures - Part 1 Experimental", *Proceedings of the 19th Australian Wind Engineering Workshop.*

Patankar, S.V., 1980, "Numerical Heat Transfer and Fluid Flow", Taylor and Francis.

Scikit-learn developers, 2017, Python SciKit Learn 0.18.2 Linear Models.